Core–Shell Pure Collagen Threads Extruded from Highly Concentrated Solutions Promote Colonization and Differentiation of C3H10T1/2 Cells

Lise Picaut, Lea Trichet, Christophe Hélary, Guillaume Ducourthial, Marie-Ange Bonnin, Bernard Haye, Olivier Ronsin, Marie-Claire Schanne-Klein, Delphine Duprez, Tristan Baumberger, et al.

Core-shell pure collagen threads extruded from highly concentrated solutions promote colonization and differentiation of C3H10T1/2 cells

Authors: Lise Picaut[1,2], Léa Trichet[2], Christophe Hélary[2], Guillaume Ducourthial[3], Marie-Ange Bonnin[4], Bernard Haye[2], Olivier Ronsin[1], Marie-Claire Schanne-Klein[3], Delphine Duprez[4], Tristan Baumberger[1] and Gervaise Mosser[2].

Affiliations :

1 Institut des Nanosciences de Paris, Sorbonne-Université, UPMC Univ Paris 6 and CNRS-UMR 7588, F-75005 Paris, France,
2 Sorbonne-Université, Laboratoire de Chimie de la Matière Condensée de Paris, UPMC Univ Paris 6, CNRS-UMR 7574, F-75005 Paris,
3 Laboratoire d'Optique et Biosciences, Ecole Polytechnique, CNRS, INSERM, IP Paris, F-91128 Palaiseau, France
4 Sorbonne Université, CNRS, Institut Biologie Paris Seine, IBPS-UMR 7622, Developmental Biology Laboratory, Inserm U1156, F-75005 Paris, France

Corresponding author: Gervaise.Mosser@upmc.fr

Abstract

The elaboration of scaffolds able to efficiently promote cell differentiation towards a given cell type remains challenging. Here we engineered dense type I collagen threads with the aim of providing scaffolds with specific morphological and mechanical properties for C3H10T1/2 mesenchymal stem cells. Extrusion of pure collagen solutions at different concentration (15, 30 and 60 mg/mL) in a PBS5X buffer generated dense fibrillated collagen threads. For the two highest concentrations, threads displayed a core-shell structure with a marked fibril orientation of the outer layer along the longitudinal axis of the threads. Young modulus and ultimate tensile stress as high as 1 MPa and 0.3 MPa, respectively, were reached for the most concentrated collagen threads without addition of any cross-linkers. C3H10T1/2 cells oriented themselves with a mean angle of 15° - 24° with respect to the longitudinal axis of the threads. Cells penetrated the 30 mg/mL scaffolds but remained on the surface of the 60 mg/mL ones. After three weeks of culture, cells displayed strong expression of the tendon differentiation marker Tnmd, especially for the 30 mg/mL threads. These results suggest that both the morphological and mechanical characteristics of collagen threads are key factors in promoting C3H10T1/2 differentiation into tenocytes, offering promising levers to optimize tissue engineering scaffolds for tendon regeneration.

Key words: Collagen, Extrusion, SHG, tendon, differentiation

Introduction

Tendons are dense connective tissues transmitting the forces developed during muscle contraction to the bones. They are mainly composed of an extracellular matrix, which major constituent is type I fibrillar collagen. The mean orientation of these collagen fibrils corresponds to the main axis of the tendon. This anisotropy is found at multiple length scales through a fibrillar hierarchical organization [1]. Tendons are prone to acute or chronic pathologies, also referred to as tendinopathies. Even though intrinsic factors are frequently involved, tendinopathies are often secondary to overuse or overload [2]. For example, most of the acute Achilles tendon ruptures, which occur at an annual incidence rate estimated between 5.5 and 18/100,000 [3], are secondary to sports activities. Acute tendon injuries can also be secondary to trauma, including lacerations by a sharp object.

Tendons present limited spontaneous regenerative capacity and high rate of re-injury mostly because of their low cellularity and their poor vascularization. Current clinical strategies to repair tendon include sutures, metallic implants, synthetic grafts and auto-, allo- or xenografts [4–6]. Autografts show the best results as surgical procedures are now less invasive and highly sophisticated [7]. However, partial removal of patient tendon is needed and can lead to morbidity of donor sites [8]. To overcome such issue, tissue engineering strategies arise and new materials are currently emerging such as tendon-like scaffolds either made of synthetic polymers (PGA, PLA, PCL) [9] or biocomponents (natural/organic components) including polysaccharides [10], collagen [11,12], gelatin associated with polycaprolactone [13], silk [14]. Other developments make use of scaffold free strategies [15] or *in vivo* synthesis [16].
From the perspective of mimicking tendons, the choice of the raw material is crucial and type I collagen - the tendon major component – seems a perfect candidate. Collagen scaffolds can be elaborated in a great variety of shapes (threads, tubing, sponges, sheets, 3D constructs) through different techniques [6,17]. However, to obtain materials with linear and fibrillar organizations close to those of tendons, fiber fabrication technologies have been preferred and extrusion [18], electrochemical alignment [19], 3D printing [20] and freeze casting [21] are very promising strategies for tissue engineering.

Extrusion processes are commonly used and can be easily implemented to provide meters of material per hour [11]. Threads can then be gathered and braided to form constructs at a higher level/scale with better mechanical properties than the elementary unit [22]. This bottom-up approach provides cells with both a chemical and biophysical environment mimicking the extracellular matrix of native tendons and the hierarchical structure of collagen assembly. Stimulation of cell proliferation and differentiation is then expected to further improve the structural and mechanical properties of the scaffold. However, the produced scaffolds have to be mechanically suitable for the grafting at the injury site and to be stable over time to avoid early degradation by the patient cells or calcification [17,23]. Native tendons exhibit remarkably high values of the Young's modulus and Ultimate Tensile Strength (UTS), respectively reaching 1.9 GPa and 120 MPa [14]. Scaffolds with such high Young's modulus and UTS have not been reported in wet conditions yet and if so, only by using post-processing steps such as

chemical cross-linking, drying etc. The impact of those treatments on cell adhesion, proliferation or migration are still controversial [6,15,17,21], questioning the relevance of such post processing techniques.

Previous reports on collagen gels have shown that the higher the collagen concentration the higher the mechanical properties [24] of collagen scaffolds. In a different context, it was also shown that although osteoblasts could not colonize collagen scaffolds at 40 mg/mL *in vitro,* they actually did it *in vivo* [25]. This approach has yet never been tested in the case of threads and in the context of tenocyte differentiation.
In another previous report, we analyzed the effect of the fibrillogenesis buffer on the stability and quality of threads synthetized at 60 mg/mL[26]. In the present work, we synthetized pure collagen threads at different concentration (15, 30, 60 mg/mL) in the buffer previously selected (PBS5X), using a homemade extruding apparatus[26,27], without any post processing steps. We thoroughly characterized the structural and mechanical properties of these threads in DMEM cell culture buffer and in the PBS5X control condition. To check for tenocyte differentiation, we used the C3H10T1/2 cell line and analyzed its behavior and cell differentiation over three weeks of cell culture.

1. Materials and methods

1.1 Collagen type I preparation

Type I collagen was extracted and purified from young Wistar or Sprague-Dawley rat tail tendons as previously described [26]. Briefly, after selective precipitations of collagen 0.6 M NaCl, the final collagen pellets were solubilized in 500 mM – pH=2.5 acetic acid and thoroughly dialyzed against the same solvent up to complete salt removal. The resulting solutions were kept at 4 °C and centrifuged at 41,000×g (Beckman Coulter J26-XP) for 4 h prior to using. Sample purity was assessed by SDS-PAGE electrophoresis and collagen concentration was determined by hydroxyproline titration.
Collagen solutions were concentrated at 10°C with centrifugal filtration units (Vivaspin®, Sartorius, with a 100 kD cutoff) at 3000×g, until reaching the desired final concentrations (15, 30 or 60 mg/mL). Solutions were then placed in 1 mL syringes and air bubbles degassed by centrifugation at 3000×g for 30 min at 10°C.

1.2 Extrusion of dense collagen solutions, fibrillogenesis and maturation

1 mL syringes filled with acidic collagen solutions (15, 30, or 60 mg/mL) were mounted with a 23-gauge (inner diameter of 390 µm) blunt stainless-steel needle. The syringes were loaded vertically on a home-made extrusion set-up [27] and solutions were extruded into a fibrillogenesis buffer (PBS 5X – pH 7.4) at an output velocity at the needle tip of V= 3.5 ± 0.5 mm/s as already described [26]. 0.3 mL of collagen were extruded in 65 mL of PBS 5X - pH 7.4. This buffer was chosen based on a previous study [26]. We define the average shear rate in the capillary as: $\dot{\gamma}$ = V/R with R the capillary radius and V the velocity of the thread.
At the blunt needle exit, extruded threads, plunging into the fibrillogenesis bath, were observed and monitored by a camera through an optical window. Prior to use, the threads

were kept in fibrillogenesis buffer (PBS 5X) for 2 weeks at room temperature under gentle agitation to achieve maturation while preventing thread surface adhesion. The thread diameters (D) were measured by optical microscopy immediately after extrusion and then regularly over the whole period, on at least three different areas of each thread. 15 mg/mL threads revealed difficult to handle during the course of the study and thus no values are reported here. The swelling ratio D/D_0 was then calculated as the ratio of the measured diameter D and the inner diameter of the extrusion needle (D_0). 4 to 5 measurements were made for each concentration (30 mg/mL and 60 mg/mL). The mean values are represented with the Pearson standard deviations.

1.3 Mechanical tests

Mechanical tests were performed using a BOSE® ElectroForce® 3200 Series II Test Instrument as already described [26]. Sample and crossheads were immersed in a glass Petri dish filled with fibrillogenesis buffer at room temperature. Initial thread diameter, D_i, was determined by optical microscopy assuming full cylindrical symmetry. Mechanical loading of the thread was achieved by driving one crosshead at a constant velocity of 0.1 mm per second with a stepping motor (0.1-micron steps). The loading force F was measured with a 220g load cell. We defined the nominal tensile stress as $\sigma = 4F/\pi D_i^2$. The nominal strain was defined as $\varepsilon = (L-L_0)/ L_0$, where L is the distance between the glue points and L_0 its initial value when the thread is straight, in its unstressed reference state. All measurements were performed up to rupture on at least 4 samples. The resulting stress-strain curves were plotted and analyzed. For each concentration N different threads were tested: N=10 for collagen threads at 30 and 60 mg/mL and N=4 for collagen threads with cells. The lower number of threads with cells tested is due to technical drawbacks as discussed below. The initial « toe » of the σ (ε) curve ($\varepsilon \leq 2\%$) is an artefact corresponding to the straightening of the residual/remaining thread deflection. The Young modulus and UTS are respectively determined as the slope $d\sigma/d\varepsilon$ of the linear regime (typically, $2\% < \varepsilon < 5\%$) and as the maximum stress of the σ (ε) curve.

Data were analyzed using GraphPad Prism 5.0 (GraphPad Software), by an unpaired Student's t test and by Tukey's test for data of the same or different group respectively. Statistical significance was set at $^*P < 0.05$, $^{**}P < 0.01$, and $^{***}P < 0.001$.

1.4 Cells culture on threads

The same culture medium was used for all the experiments with the murine mesenchymal stem cell line C3H10T1/2 [28] (ATCC CCL – 226). The cells were first cultured in proliferation conditions in 250 mL flasks at 37°C, 5% CO_2, in 1 g/L glucose DMEM medium (Sigma-Aldrich, St. Louis, MO, USA) complemented with 10% of Fetal Bovine Serum (Gibco Invitrogen, Waltham, MA USA), 2% of penicillin-streptomycin (Gibco Invitrogen, Waltham, MA, USA) and 2% of 200 mM L-glutamine (Gibco Invitrogen, Waltham, MA, USA). Cells were harvested at 90% confluence. Passages 18 to 23 were used for experiments.

Matured threads kept in PBS 5X- pH7.4, threads were cut into segments of about 2 cm length and pinned 10 mm apart on already prepared SYLGARD silicon gel-covered wells (Dow Chemical, Midland, MI, USA) with two 8 mm sutures (Ethican, Sommerville, NJ, USA) as

adapted from Kapacee *et al.* [29] (see Fig. SI-1). The threads were rinsed and soaked into DMEM for several days to check for absence of contamination. The DMEM was changed again extemporaneously to cell culture. Each collagen thread was seeded with 2 mL of culture medium with 750 000 cells and placed to incubation conditions. Control collagen threads without cells were also monitored. Culture medium was renewed every two days. After 2 weeks, in order to proceed with further investigations, collagen threads were retrieved and fixed in PBS solution containing 4% paraformaldehyde. Cell culture series of at least 12 threads for each collagen concentration was repeated 3 times.

1.5 In situ hybridization to collagen

Threads with cells were fixed overnight in 4% paraformaldehyde solution diluted in PBS, embedded in paraplast, and sectioned at a thickness of 8 µm with a microtome (Microm). *In situ* hybridization was then performed as previously described [30]. The digoxigenin-labeled mRNA mouse probes were used as previously described: Myod [31], Col1a1 [32], Scx and Tnmd [33]. The experiments were repeated 3 times for each concentration. For each concentration, sections were photographed on two different areas using an optical microscope.

1.6 Microscopy analysis

For optical analysis, threads were put in home-made glass-chambers filled with PBS 5X to prevent dehydration during observation. Polarized light microscopy was performed using a transmission Nikon Eclipse E600 Pol, equipped with crossed polarizers, a quartz first order retardation plate and a DXM 1200CCD camera.

Multiphoton imaging was performed using a custom-built upright microscope combining second harmonic generation (SHG) and two-photon excited fluorescence (2PEF) modes of contrast as previously described [34]. SHG was used because it reveals specifically unstained fibrillar collagen. The excitation was provided by a femtosecond titanium-sapphire laser (Mai-Tai, Spectra-Physics) set at 860 nm. A circular polarization was used to image collagen fibrils independently from their orientation in the focal plane. The collagen threads were imaged using a 20 x 0.95 NA objective with a lateral resolution of 0.6 µm and an axial resolution of 3.5 µm. Power at focus was typically 85 mW, with 10 µs pixel dwell time. 2PEF was epi-detected and SHG was epi- and trans-detected using three channels equipped with photomultiplier Tubes (P25PC, SenTech) and appropriate spectral filters. Unlabeled samples were imaged in observation chambers filled with fibrillogenesis buffer.

Image analysis was performed using ImageJ software (NIH) to determine the main orientation of the fibrillar structures in the peripheral regions of the threads (shells). Automatic particle analysis was conducted after manual thresholding of longitudinal midsections of three different threads at 60 mg/mL and two different threads at 30 mg/mL. At least 265 different regions of 9 to 175 µm² were analyzed for each condition. The angles corresponding to the fitted ellipses were then averaged.

Multiphoton microscopy was also used to image collagen threads with fluorescently-labelled cells. For fluorescent labeling, collagen threads with cells already fixed in PFA 4% solution were immersed in 0.2% Triton X-100 for 15 min. After several rinsing with PBS solution, Alexa Fluor 488 Phalloidin was put on samples left in the dark at 4˚C. PBS rinsing stages

were then needed to remove Alexa excess. Finally, the DAPI solution was added during 15 min and rinsed again before imaging.
SHG was trans-detected as above, and 2PEF signals were epi-detected in two different channels using a dichroic filter (Di02-R488, Semrock).
Image analysis was performed using Matlab (Mathworks), ImageJ (NIH) and Imaris (Bitplane).

For scanning electron microscopy (SEM), the samples were prepared as already described (fixation, dehydration, freeze drying and gold sputtering (20 nm) [26]. The samples were observed on a Hitachi S-3400N SEM operating at 3 kV. For transmission electron microscopy (TEM), samples were prepared as already described [26]. Embedded samples were sectioned on a Leica EM UC7. 70 nm ultrathin sections were contrasted with uranyl acetate and observed on a FEI Tecnai spirit G2 operating at 120 kV. Images were recorded on a CCD Camera (Orius Gatan 832 digital).

1.7 *Quantification of cells number per surface unit area and of their alignment on the thread.*
Combined 2PEF/SHG images were used to locate the threads through their SHG signal and assess the features of the cells lying on these threads through their fluorescent labeling, either Dapi for nuclei or Alexa Fluor 488 Phalloidin for actin filaments.
The cell densities on the threads were estimated by counting the number of cells nuclei per mm^2 with ImageJ on 2 regions of interest (300 µm x 300 µm) for threads at 30 and 60 mg/mL collagen concentrations. The central area was chosen to be approximately two thirds of the thread width.
The main orientation of the cells on the threads were obtained from Alexa Fluor 488 Phalloidin images using Orientation J plugin. Four different threads were analyzed for each condition at 30 and 60 mg/mL. Gaussian fits of the distributions of orientation were performed. Full widths at half maximum ranged between 35 and 55°, and for each condition the orientations corresponding to the peaks of the Gaussian fits were averaged to assess the main orientation.

1.8 Quantitative reverse transcription polymerase chain reaction (RT-q-PCR)

Collagen threads were taken out from cell culture wells and immersed in 1 mL of TRIzol solution (pH 6). Then, threads were scrubbed with a cell scraper to insure collecting RNA from cells that had penetrated the matrices. The supernatants were collected into cryotubes and stored at -80°C until used. After thawing and a centrifugation at 10000 g to eliminate remaining aggregates, 0.2 mL chloroform was added to the collected supernatants. The upper phase containing RNAs was then collected and purified using an RNeasy mini kit (Qiagen, France). The RNA concentration and purity were evaluated by absorbance measurement at 260 nm and 280 nm. RNAs were then reverse transcripted into complementary DNA (cDNA) using random primers and MMLV RT enzyme (Life Technologies) at 37°C. Real time PCR amplifications of Col1a1, TnmD and Scx were performed with a Light Cycler 480 (Roche) using selected primers (Table S1) and Sybr Green chemistry. For this purpose, a Light Cycler 480 SYBR green I master kit (Roche) was used. Cycling conditions were: initial Taq

polymerase activation at 95°C for 5 min followed by 40 cycles, each cycle consisting of 30s denaturation at 95°C, 50s annealing at 59°C and 45s elongation at 72°C. Then, a melting curve was obtained for each gene by increasing the temperature from 60 °C to 97 °C at a rate of 0.1 °C/s to assess the reaction specificity. The results were analyzed using a relative quantification following the Pfaffl method. For each gene, the efficiency of the target primer pairs was measured by producing a curve based on the amplification of a serial dilution of cDNA. For each target gene, the mRNA transcript level was normalized with the housekeeping gene 36B4 since its expression is not modified in our conditions. A ratio was calculated by comparison with a calibration point which was the gene expression of cells cultivated on 30 mg/mL collagen at day 7 and the value 1 arbitrary given to this calibration point.

1.9 Gene expression analysis

Statistical analysis

The gene expression results of real time qPCR are presented as the mean value ± SD (standard deviation). The statistical significance was assessed using one-way analysis of variance (ANOVA) followed by Tukey posthoc test (comparing all pairs of groups) while comparing 3 data sets. We used this test for evaluating the influence of cell culture time at 3 different times (1, 2, 3 weeks). The significance level in all statistical analyses was set at a probability of $P < 0.05$.

2. Results

Pure collagen threads were produced at 15, 30 and 60 mg/ml. They were followed over three weeks after extrusion, to check for their swelling characteristics. All other characterizations (structure, organization and mechanical properties) as well as cell culture were performed two weeks after extrusion once full fibrillogenic maturation had occurred. As described below, this allowed us to discard the condition at 15 mg/mL due to poor mechanical characteristics. Threads synthetized with the two highest concentrations were checked for their ability to sustain C3H10T1/2 cell culture and differentiation into tenocytes.

2.1 Extrusion and maturation

Just after extrusion, all threads looked white alike native tendons and their surface appearances varied with concentrations: smoothness at 15 mg/mL (Fig. 1A), roughness corresponding to a sharkskin appearance [26,35] at 30 and 60 mg/mL (Fig. 1B and C). After two weeks of maturation, 15 mg/mL threads remained smooth (Fig. 1D) and surface patterns were still observed at 30 and 60 mg/mL with depths reaching 25 and 10 µm respectively (Fig. 1E and F). This roughness was further confirmed by SEM (Fig. SI.2).

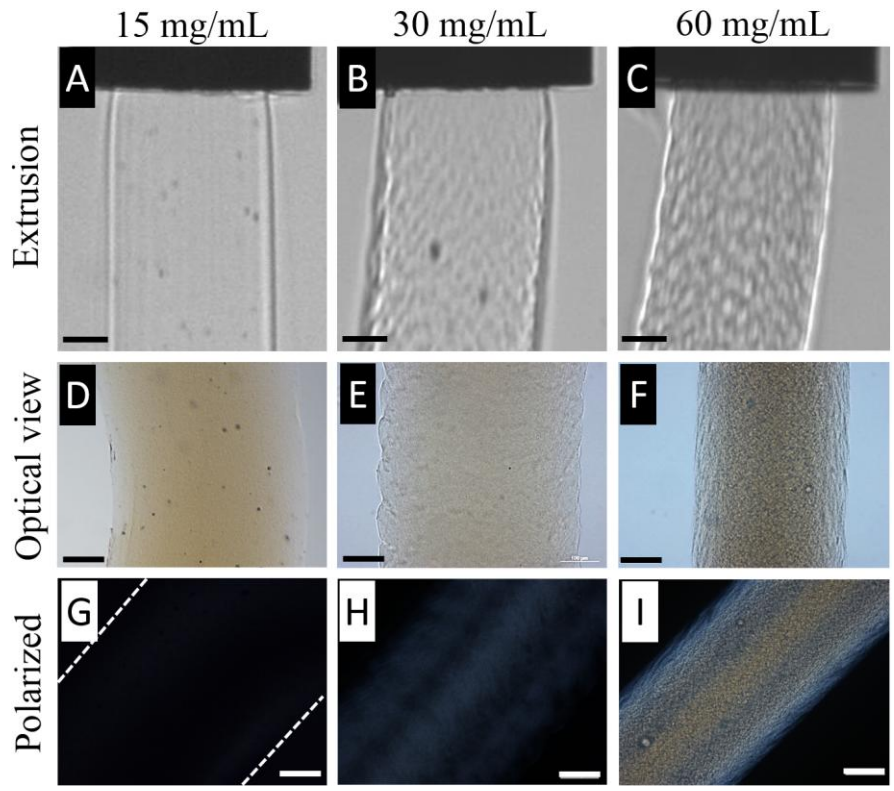

Figure 1: Collagen threads observed by different techniques at different concentrations.). During the extrusion of collagen thread at 15 mg/mL, the collagen flow is homogeneous and the thread seems to be smooth (A). The smoothness is confirmed by optical (D) and SEM (See Fig. SI-2A). At 30 and 60 mg/mL (B and C), a pattern at the thread surface is observed during the extrusion. It is also visible by optical imaging (E and F) and SEM where a periodic/regular roughness appears (See Fig. SI-2B&C). No birefringence signal is observed for collagen threads at 15 mg/mL by polarized imaging (G). Collagen threads at 30 and 60 mg/mL display respectively a low and a higher signal indicating collagen anisotropy (H and I). Scale bars are 100 µm.

Observation in between crossed polarizers with the threads positioned at 45° showed no signal at 15 mg/mL (Fig. 1G) while a bright signal appeared along the threads' axis at 30 and 60 mg/mL (Fig. 1H and I) with an increased intensity at 60 mg/mL. During the maturation time, the diameters of the threads at 15 and 30 mg/mL became wider while those at 60 mg/mL remained constant as shown by the evolution of the diameters over time for the different conditions in the fibrillogenesis buffer PBS 5X (Fig. 2). For each concentration, threads diameter evolved within the first four days and then reached a plateau. We found that threads at 15 and 30 mg/mL systematically swell ($D/D_0>1$) while those at 60 mg/mL exhibit a D/D_0 remaining close to 1 even after 2 weeks of maturation. The threads mean diameters at day 18 were 519 ± 28 µm, 498 ± 10 µm and 390 ± 5 µm at 15 mg/mL, 30 mg/mL and 60 mg/mL respectively.

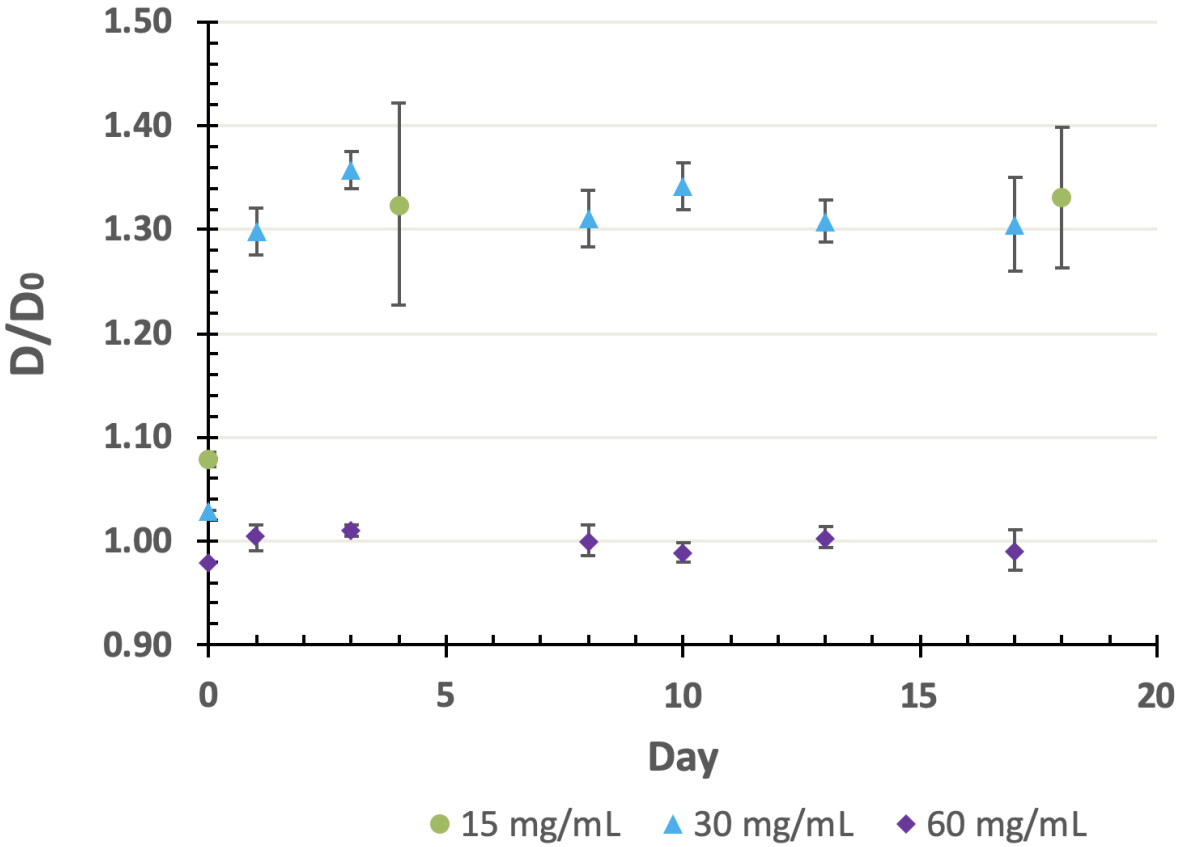

Figure 2: Evolution of collagen threads diameter over time. The ratio of the measured thread diameter D and the inner diameter of the needle D_0 was plotted as a function of the time (day) for collagen threads at 15 mg/mL (green circle), 30 mg/mL (blue triangles) and 60 mg/mL (purple rhombs). This ratio increases within the first days for the lowest concentration and remains constant for the highest one. After 3 days of maturation, collagen threads diameter is stable for all conditions.

2.2 Structural characterization

2.2.1 Transmission electron microscopy

The threads were analyzed by transmission electron microscopy (TEM) at low and at high magnification (Fig. 3, resp. left and right). We observed the distribution of the fibrils as well as their morphology. In all threads, fibrils presenting the typical collagen 67 nm cross-striation were observed. The diameter of the fibrils was about 40-60 nm and their lengths were greater at 15 mg/mL and 60 mg/mL reaching at least 1 µm. They appeared thinner at 30 mg/mL. Fibrils cut perpendicular to their axis, give the dotted features, and fewer appeared cut along their longitudinal axis. At 60 mg/mL, the compaction of the fibrils, clearly visible, induces some local wavy organizations Fig. 3E).

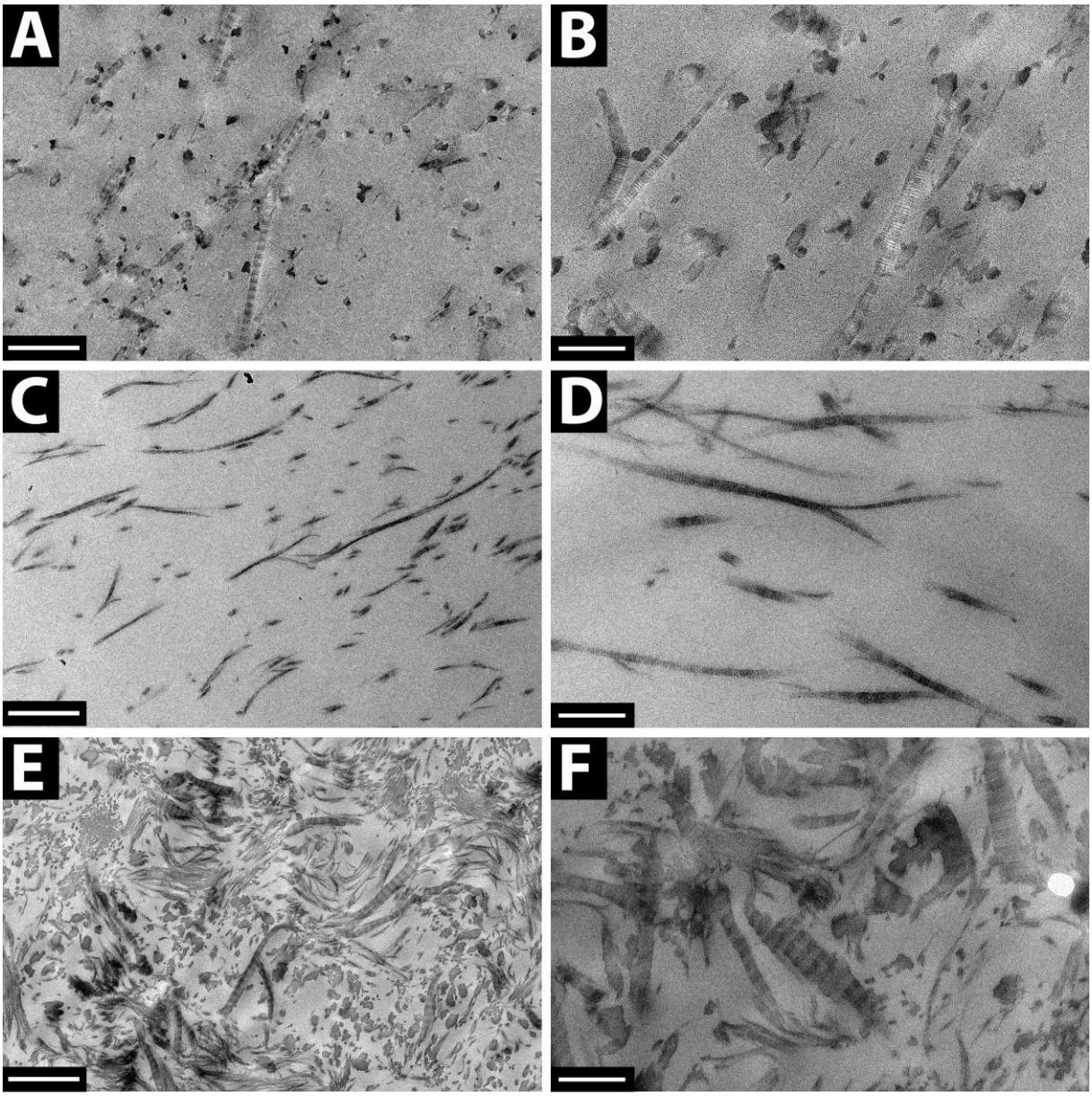

Figure 3: Ultrastructure observations by Transmission Electron Microscopy (TEM) of collagen threads after 2 weeks of maturation in PBS 5X (transverse sections). Figures A&B, C&D, E&F, correspond respectively to collagen threads at concentrations 15, 30 and 60 mg/mL. Collagen fibrils appear cut in all directions from longitudinal to transverse, in which case they appear as dots. In all threads, fibrils presenting the typical collagen 67 nm cross-striation are observed. Scale bars: left, 500 nm, right, 200 nm.

2.2.2 Second Harmonic Generation Microscopy

Figure 4 displays the collagen threads as observed by Second Harmonic Generation microscopy (SHG). At lower magnification (Fig. 4A1), SHG intensity was homogeneous in every direction at 15 mg/mL. At 30 mg/mL, over a distance of about 50 µm from the surface, tilted black stripes were observed delineating a cylindrical shell (Fig. 4B1). The inner thread core looked unstructured. At 60 mg/mL, the same features were observed, yet more pronounced, and over a distance of about 100 µm (Fig. 4C1). More precisely, at day 14, when the thread was stabilized, we found that the shells represented 31% and 53% of the whole diameter respectively at 30 and 60 mg/ml, (s.d. of 6% and 4% respect.). A radial symmetry of

the shell structuration was clearly visible (Fig. 4, ABC-2) with angular variation of fibrillar structures at the core-shell junction. The mean angle in the shell was measured as 14° (SD=39°) and 6° (SD= 41°) from the central longitudinal axis of the threads at 30 and 60 mg/mL respectively. The core-shell interface was characterized by a lower SHG signal.

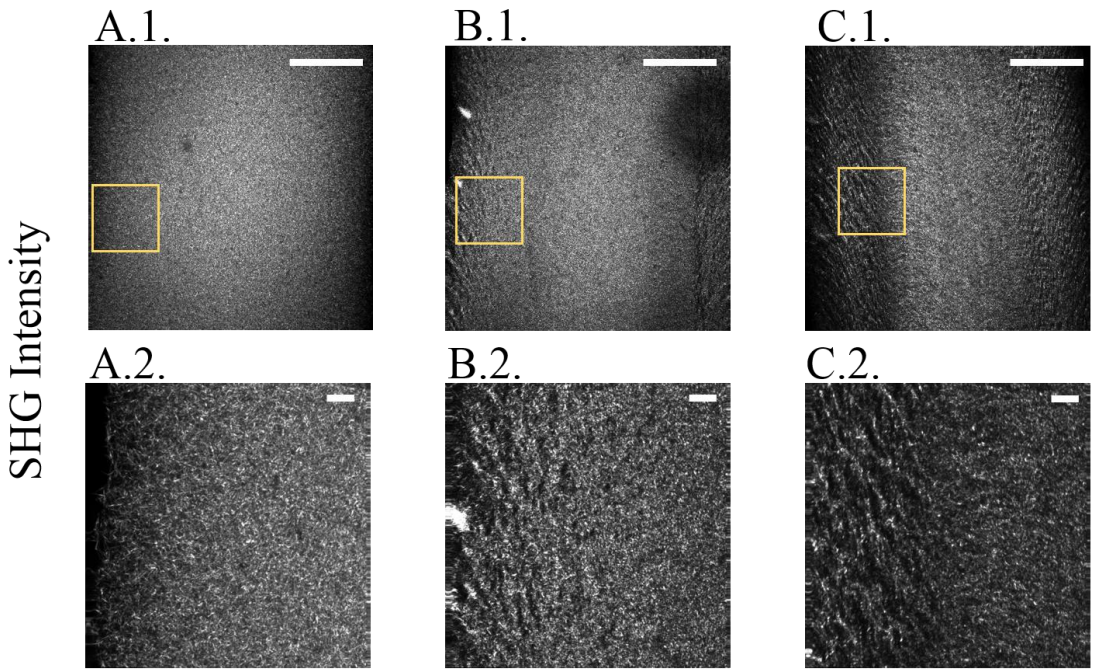

Figure 4: Second Harmonic Generation (SHG) observations of collagen threads. TOP - A.1, B.1, C.1: SHG imaging of collagen threads at respectively 15 mg/mL, 30 mg/mL and 60 mg/mL. The imaging plane corresponds to a longitudinal optical section in the thread center. The threads are placed vertically and their borders are visible on each side (left and right) of the images. Scale bars: 100 µm. BOTTOM - A.2., B.2., C.2.: SHG imaging of zoomed-in images taken in the yellow squared areas respectively in A.1., B.1., C.1. Scale bars: 10 µm.

In Fig. SI-3 an example of collagen thread at 60 mg/mL clearly shows collagen fibrils clusters at the outer surface (Fig. SI-3, top left 1) as already observed by SEM (Fig. SI-2). We noticed several concentric "layers" from surface to center (Fig. SI-3, top right 2). A transverse reconstruction rendered the cross-section thread organization (Fig. SI-3 bottom).

2.3 Mesenchymal stem cell behaviors on threads

Threads at 15 mg/mL were so fragile that both mechanical testing and cell culture was not possible to be carried out. This made them unsuitable for tissue engineering applications and they were therefore discarded for further investigations.

Collagen threads at 30 mg/mL (Fig. 5A) and 60 mg/mL (Fig. 5B) seeded with C3H10 T1/2 cells over 3 weeks were observed by multiphoton microscopy (Fig. 5). In both cases, cells

(Fig. 5, red color corresponding to phalloidin labeling) covered the entire surface and built up into a multilayer of about 50 µm consisting of c.a. 5 cellular layers. At 30 mg/mL, several straight regions with no SHG signal, equivalent to the size of one or two elongated cells, were observed 30 µm under the surface within the collagen threads (Fig. 5A BOTTOM). Cell labeling enabled to attribute those regions to cells. Cell density on collagen threads at 30 mg/mL and 60 mg/mL was evaluated to 1300 ± 300 cells/mm^2. At the cell sheath surface, the cell actin filaments (red) reflected the main orientation of the cells (orange arrows, Fig. 5A, B). For both types of threads at 30 and 60 mg/mL, the main orientation of the cells with respect to the thread longitudinal axis was found to be 15° ± 4° and 24° ± 6, respectively (Fig. SI-4).

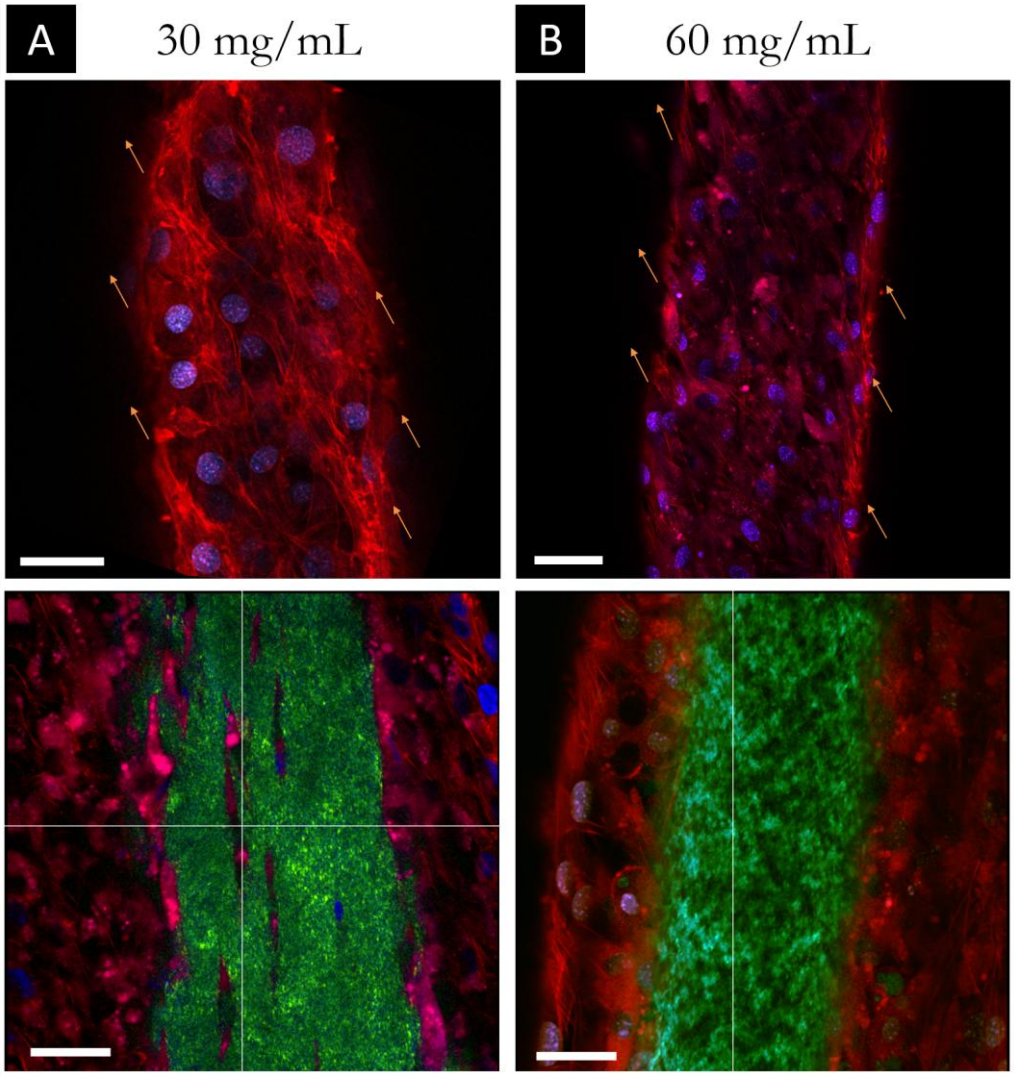

Figure 5: SHG/2PEF imaging of collagen threads at 30 mg/mL (A) and 60 mg/mL (B) seeded with C3H10T1/2 cells during 3 weeks under static load. (A&B TOP) threads surface, (A&B BOTTOM) at 30 µm depth. Green: SHG signal of collagen, Red: fluorescence from Alexa Fluor 488 Phalloidin labeling of actin filaments; Blue: fluorescence from DAPI labeling of cell nuclei. Orange arrows are eye guidelines to see the cell actin filaments main orientation. Scale bars = 50 µm.

In order to assess the differentiation state of mesenchymal stem cells (C3H10T1/2) cultured on the collagen threads for 3 weeks, tendon gene expression was analyzed by *in situ* hybridization in histological transverse collagen thread sections at 30 and 60 mg/mL (Fig. 6 & Fig. SI-5). Tendon differentiation was assessed with the expression of *Scx* (scleraxis) the key marker of tendon progenitors, *Tnmd* (Tenomodulin), the tendon differentiation marker and *Col1a1* coding for one of the type I collagen chains, the main structural and functional component of tendons [36]. The expression of MyoD (a muscle marker) was used as an internal control. In agreement with SHG/2PEF data, cells had penetrated further in the 30 mg/mL threads compared to those at 60 mg/mL (Fig. 6A), while tendon genes were expressed in both conditions (Fig. 6A, B). *Tnmd* displayed a high expression in 30 mg/mL collagen threads compared to *MyoD* expression (Fig. 6A), while the 3 tendon genes were highly expressed in 60 mg/mL collagen threads compared to *MyoD* expression (Fig. 6B).

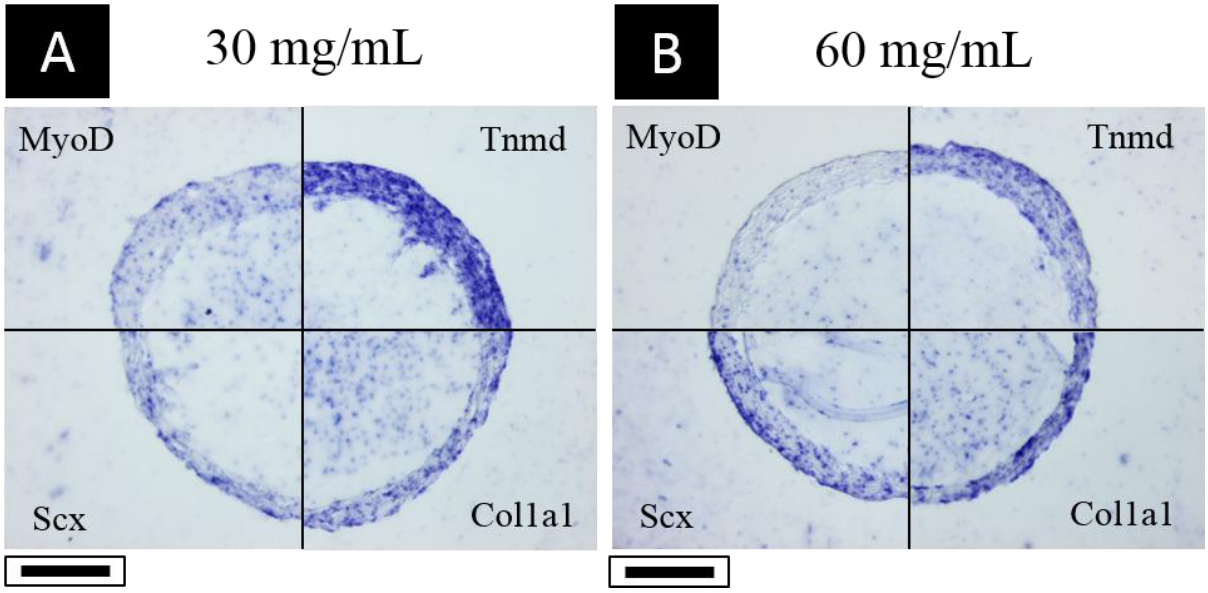

Figure 6: In situ hybridization to transverse sections of collagen threads at 30 mg/mL (A) and 60 mg/mL (B) seeded with C3H10T1/2 cells and cultured during 3 weeks. Tendon gene expression was visualized with *Col1a1* (Type I collagen), *Scx* (Scleraxis) and *Tnmd* (Tenomodulin) probes. *MyoD* (muscle marker) was used as a control probe. The tendon differentiation gene, *Tnmd* displayed high expression in 30 and 60 mg/mL threads. Scale bars = 100 µm.

Differentiation of cells cultured on 30 mg/ml threads was also assessed by RT-qPCR. The expressions of Col1a1, Scx and Tnmd, three phenotypic markers of tenocyte differentiation were analyzed. The expression of Scx and Tnmd decreased from day 7 to 21 while that of collagen 1 increased during this period of time (Fig. SI-6).

2.4 Mechanical properties

Tensile testing experiments were performed after 3 weeks of cell culture on collagen threads with and without cells in fibrillogenesis buffer (PBS 5X) or DMEM (Fig. 7). At 30 mg/mL, a Young Modulus (E) of about 0.20 MPa was reached (Fig. 7A) while at 60 mg/mL, the value was almost 8 times larger. The Ultimate Tensile Strength (UTS) was 4-fold higher at 60 mg/mL than at 30 mg/mL (Fig. 7B). Seeded with cells, collagen threads at 60 mg/mL exhibited better mechanical properties with E = 1.11 ± 0.30 MPa and UTS = 0.14 ± 0.04 MPa than those at 30 mg/mL for which the Young modulus was almost 10-fold and the UTS 3-fold lower (Fig. 7).

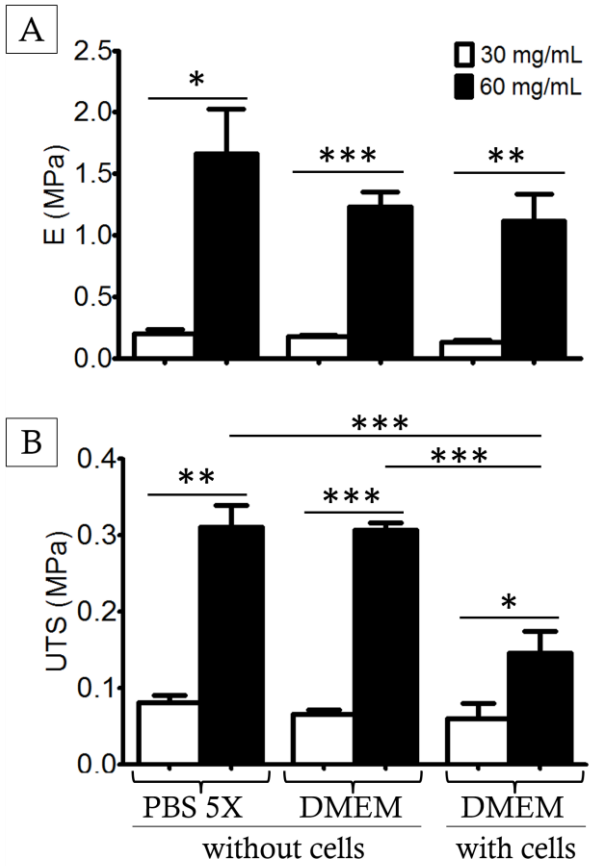

Figure 7: Result of tensile testing of collagen threads at 30 mg/mL (white) and 60 mg/mL (black) seeded with cells and cultured over 3 weeks under static load and their respective controls in absence of cells in fibrillogenesis buffer (PBS5X) and cell culture medium (DMEM). (A) Young modulus and (B) Ultimate Tensile Stress.

3. Discussion

The main objective of this work was to produce pure dense collagen threads, avoiding post-processing and chemical treatments, with appropriate mechanical properties suitable for

C3H10T1/2 cell proliferation and differentiation into tenocytes. Moreover, we chose the extrusion technique of dense collagen solution as it enables fast and easy scaling-up for the production of meters of collagen threads in a short time. In this study, three different collagen concentrations were tested: 15 mg/mL (commonly used [11,37,38]), 30 and 60 mg/mL. The collagen threads were characterized from the macroscopic scale (optical observations, diameter stability, mechanical properties) to the microscopic one (fibril size, orientation and organization). Except for the evolution of diameters right after extrusion and during three weeks, all characterizations and cell culture were made on threads having reached stability after a two-week maturation process. Indeed, preliminary unpublished experiments have shown that the use of non-matured threads gave irreproducible results when set to culture. In an altogether different study[39], optical evolutions was observed during this maturation process, which we discussed in terms of possible collagen molecules rearrangement within the scaffold.
During extrusion, we observed sharkskin instability at 30 and 60 mg/mL and not at 15 mg/mL. In Gobeaux *et al*. work [40], rheology of such concentrated solutions was studied and evidenced a newtonian plateau $\eta = \eta_0$ for shear rates $\dot{\gamma} < \dot{\gamma}_0$, and a strong shear thinning behavior where $\eta(\dot{\gamma}) = \eta_0 (\dot{\gamma}/\dot{\gamma}_0)^{m-1}$, with m=0.3. For $\dot{\gamma} >> \dot{\gamma}_0$, the ratio $\dot{\gamma}/\dot{\gamma}_0$ quantifies the viscoelasticity of the solution [41]. Sharkskin is a response of viscoelastic fluid to the strong (singular) elongational stresses occurring in the exit region. We conclude that at the shear rate imposed here, $\dot{\gamma}$ = 4.5 s^{-1}, collagen solutions at 30 and 60 mg/mL are in the strong shear-thinning region whereas solutions at 15 mg/mL are almost at the end of the newtonian plateau. This explains why we do not see sharkskin instabilities at 15 mg/mL in collagen. To reach these instabilities regime at such a low concentration, we would need to considerably increase the extrusion velocity.

The sharkskin surface instabilities observed after extrusion were correlated with the structures looking like clusters of collagen fibrils on threads at 60 mg/mL as observed both by SHG (Fig. SI-3) and SEM (Fig. SI-2). For the lowest collagen concentration, the surface perturbation was smaller resulting only in less pronounced pleated patterns (Fig. SI-2).

The signals observed by polarized light microscopy indicate that at least the threads at 30 and 60 mg/mL present an overall anisotropic organization. The absence of signal at 15 mg/mL is due to the low concentration. Indeed, the lower the concentration the lower the signal is and the faster molecular relaxation occurs, which further contributes to signal drop. The SHG images revealed more accurately the organizations of the threads.

The most obvious feature was a core-shell structure more pronounced with increased collagen concentration. At 60 mg/mL, this shell presented a thickness of 120 µm ± 17µm while at 30 mg/mL the thickness of the shell was limited to 79 µm ± 21µm. The core-shell limit was correlated to a lower birefringence signal and to an abrupt change in collagen fibrillar orientation (Fig. 4 C1, Fig. 8 & Fig. SI-3). We thus observe three striking effects upon extrusion and fibrillogenesis, depending on collagen concentration: - 1 – the difference in shell thickness, - 2 – the change of orientation of the fibrillar material, - 3 – the absence of SHG signal at the transition.

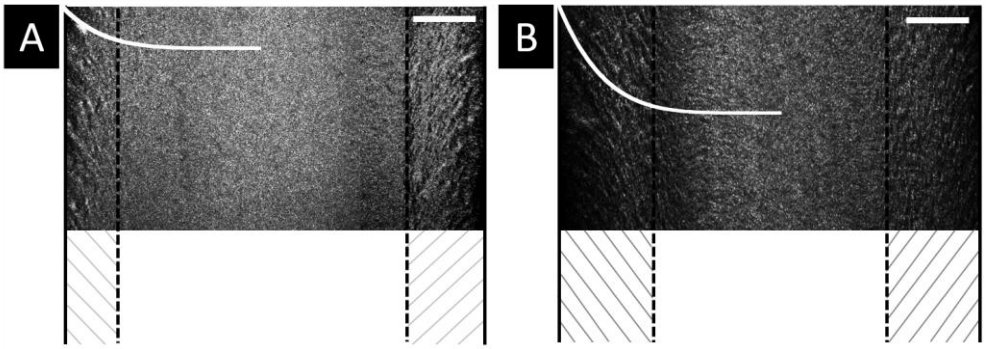

Figure 8: SHG analysis. Threads center longitudinal sections for 30 mg/mL (A) and 60 mg/mL (B). TOP: SHG images; White curves on SHG images correspond to the velocity gradient profiles (see text) plotted using the same vertical scale (arbitrary units). Scale bar: 50 µm. BOTTOM: Schemes of collagen main fibrillar orientation as revealed by the SHG images.

We believe that the first two points can be explained respectively by the rates of flow and of fibrillogenesis as follows:

-1 - Note that due to the strong shear-thinning rheology of concentrated collagen, the flow used to extrude the collagen solutions was a quasi-plug one. Accordingly, strong shear rates were localized in a near wall region. Fig. 8 showed the velocity gradient profile (power-law shear thinning viscosity $\eta \sim \dot{\gamma}^{(m-1)}$ with exponent m = 0.3 as measured by Gobeaux et al. [40]) superimposed to the SHG picture. We see, that the effect was stronger at 60 mg/mL going deeper into the thread than at 30 mg/mL explaining the difference of thickness of the shell.

-2 – Concerning the orientations found in the shell, they were compatible with the trend of collagen molecules to align along the flow direction under the rotating effect of the velocity gradient. Beside these complex fluid dynamics, we must also consider the speed at which fibrillogenesis takes place versus the speed of relaxation of the solution. In this protocol, fibrillogenesis took place in a diffusion process from the exterior to the center of the threads. The shells of the matrices, "frozen" in the high strain state, could not relax, explaining the difference of the orientation angle between the shell and the core at the two concentrations. Noteworthy, other parameters such as a swelling during the maturation process could also be taken into consideration especially at 15 and 30 mg/mL.

-3 - Thus the organization of the collagen fibrils within the threads was rather complex with changes of orientation from shell to core. The junctions between core and shell were characterized by an absence of SHG signal (Fig. SI-3). This fact indicated that this limit could either be an area depleted in collagen or an area where collagen molecules presented “antiparallel” or “random” organizations.

Regarding the TEM data, the fact that we observed thinner fibrils at 30 mg/mL than at 15 and 60 mg/mL likely relies on the strong relationship between the viscosity of the collagen solutions and the final fibrils dimensions as we previously reported [40]. In the mentioned work,

we showed that there were four different concentration ranges with non-monotonous growth of fibrils. The four regions stood from approximatively 0.1 to 6, 6 to 20, 20 to 200 mg/mL and above, with corresponding increase, decrease, increase and decrease of fibril dimensions. It is possible that the four ranges of concentrations indicated in our former work would have been impacted and shifted by the extrusion process, thus explaining the non-linear variation of fibrils dimension with increased collagen concentration. Due to experimental issues, we were unfortunately not able to get longitudinal sections or break the threads to see the shell and core and the change of orientation by TEM or SEM respectively. However, the SHG signal clearly shows this change at micrometer resolution.

Concerning the mechanical properties of our dense collagen threads, significant differences were noticed for Young Modulus (E) and Ultimate Tensile Strength (UTS) in both cases between collagen threads at 30 and 60 mg/mL: the higher the collagen concentration the higher the Young modulus and the Ultimate Tensile Strength (UTS), whether the fibrillogenesis was done in buffer (PBS 5X) or in culture medium (DMEM). The 15 mg/mL threads showed too small Young modulus and UTS and were therefore discarded at this point of the study. This increase of mechanical strength with increasing concentration could be explained by an increase of density in collagen but also by the alignment of fibrils along the thread axis. The only significant decrease concerned the UTS of collagen threads at 60 mg/mL when comparing seeded threads with non-seeded ones.

Since threads made at 15 mg/mL were mechanically too weak to be handled and used for cell culture, cell behavior was only tested with threads made of 30 and 60 mg/mL of collagen. Our results clearly showed that cells adhered and proliferated on the surface of the threads at both concentrations. Cells aligned with a mean angle of 15-24° to the thread axis. Still, the load was negligible corresponding to a static strain of 0.16%, which order of magnitude was small compared to those commonly applied (about 1%) as in Kuo *et al.* study [42]. In addition to these two factors, cell orientation could also be related to an optimized curvature of the microenvironment [43]. Interestingly enough, the analysis was performed on the upper most layer, suggesting that the cells could transfer some topotactic information through the different cell layers.
Concerning the penetration and colonization of the threads by the cells, we observed a clear collagen concentration effect with cells penetrating over 30 µm in the 30 mg/mL threads, whereas they stayed on the surface of the 60 mg/mL threads. Indeed, at 30 mg/mL, combined SHG/2PEF imaging revealed cells within regions devoid of SHG signal, thus of collagen. Helary *et al.* clearly showed that cells digested collagen matrices thus creating three-dimensional routes into which other cells could penetrate [44]. The fact that such “holes” were not observed on collagen threads in absence of cells indicated that similar processes were undergoing in our present study. Besides, Helary *et al.* also showed that *in vitro,* the higher the concentration the slower was the penetrating process. This probably explains why the cells have not penetrated the 60 mg/mL threads at the same time point. The high density of collagen and high stiffness of the thread at 60 mg/mL could explain this result.

In situ hybridization showed that the C3H10T1/2 mesenchymal stem cells expressed key tendon markers after culture on collagen threads at 30 or 60 mg/mL. The tendon differentiation marker *Tnmd* was highly expressed, suggesting that collagen threads at 30 or 60 mg/mL induces the differentiation of C3H10T1/2 cells towards a tenocyte phenotype rather than that of muscle cells. The analysis of the gene expression by RT-q-PCR shows that the CH3H10T1/2 cells express Scx, Tnmd and collagen1a1 at week one. At longer cell culture time, the Scx and Tnmd expression drop while that of collagen increases. Nevertheless, RNAs resulting of the Scx and Tnmd gene expression were detected by *in situ* hybridization after 3 weeks, thereby suggesting collagen threads triggered a strong cell differentiation into tenocytes still detected at three weeks. Noteworthy, *in situ* hybridization also reveals that whether in the sheath around or penetrated in the threads, cells show a strong differentiation. The profile of differentiation is similar to that of C3H10T1/2 cells cultivated within fibrin hydrogels except for the collagen expression[45]. Hence, collagen threads allow for a sustainable collagen I expression by cells. As a result, these cells adopt a biosynthetic profile required for tendon regeneration. Note that although the cells were used at passage 18 to 23, they were still able to differentiate.

Finally, we observe that the mechanical properties of the threads in presence of the cells after 3 weeks of cell culture were worse than in their absence but exhibited the same trend: *ie*, the mechanical properties were better at 60 mg/mL than at 30 mg/mL. We can infer from our data that the decrease of the mechanical properties is not attributable to the DMEM buffer, since the values obtained in PBS5X and DMEM are equivalent. Besides, TEM analysis of collagen threads in PBS5X and DMEM did not reveal any variation (Fig. SI-8). Thus, the decrease observed in presence of cells could be explained by the cell sheath around the threads, which sometimes broke away in the clamping jaw region leading to some sliding of the threads during the tensile testing experiments. It could also be due to the hydrolysis and degradation by cells' metabolic activities. Whatever, these results further underline the fact that the threads are resistant enough to sustain possible degradation due to cells activity for weeks, leaving enough time for cells to differentiate and synthetize their own matrix. As is well known, situations *in vivo* and *in vitro* are different due to biological environment as well as mechanical stimulation. At this stage, the here reported data already show the potential of threads made of collagen from 30 mg/mL up to 60 mg/mL *in vitro*. It appears that, in order to achieve faster tissue regenerations, it is convenient to use the 30 mg/mL hydrogels. However, if you seeking for more stable long-life implants with slow regeneration, the 60 mg/mL hydrogels might be better off.

Limited literature was found about the mechanical properties of collagen scaffolds seeded with cells *in vitro* [46,47]. In most studies, cells were directly put inside the collagen-based constructs as opposed to our study where cells were added *a posteriori*. Thus, while comparing the results, we should keep in mind that cells may act differently when put from the outside or directly inside the collagen scaffold. Gentleman *et al.* made collagen threads at 10 mg/mL and used a post extrusion process of dehydration and cross-linking to improve their mechanical properties [48]. These collagen fibers (N=50) were further embedded in a cell-laden

collagen gel (2.77 mg/mL) and cultured under static load during 25 days, and then tested for tensile properties until failure. The authors compared the tangent moduli and found that the moduli of the cell-laden constructs were almost 1.7-fold higher than the ones without cells (49.6 and 83.4 MPa respectively). In this case, cells improved the mechanical properties of the constructs. We must bear in mind that cross-linking agents and braiding steps were used as post-processing in this study, which explains that the mechanical properties are better than in the present study. Kim *et al*. used 3D bioprinting to fabricate collagen-based constructs at 40 mg/mL that were cross-linked with tannic acid and laden with cells. In the case of pure cell-laden collagen scaffolds, they obtained Young's modulus of 0.04 MPa [46]. They assumed that this low value, for a collagen concentration of 40 mg/mL, was due to the mesh structure of their constructs. Indeed, this value is 3-fold lower than the one we obtained at 30 mg/mL in this present study. Chen *et al*. also produced cell-laden collagen constructs with no post-processing but with another shape (rings) and at collagen concentrations ranging from 0.5 to 2 mg/mL [47]. In contrast to our present data, they showed that the Young's modulus and UTS decreased while increasing the collagen concentration of their cell constructs. However, the collagen concentration range at which they worked was much lower than ours and the comparison is thus not straightforward. Their highest values of Young's modulus and UTS (≈ 80 kPa and ≈ 35 kPa respectively) were obtained for a collagen concentration of 0.5 mg/mL and are twice as low as those of our collagen threads produced at 30 mg/mL. More recently, Rieu and co-workers published a work on pure collagen freeze casted samples and achieved in absence of cells a Young's modulus of 33 ± 12 kPa and a UTS of 33 ± 6 kPa for an initial concentration of collagen of 40 mg/mL. Those values are much lower compared to those in our study. This could be due to the formation of smaller fibrils due either to porous material or to increased concentration upon the freezing process. However, the latter would be counterintuitive considering previous reports and our present data that mention that the higher the concentration, the higher the mechanical properties. Whatever the reason, the comparison seems to indicate that mechanical properties are better in a full thread at lower concentration with large fibrils than a porous thread at higher concentration and small fibrils. Together those data give hints of improvements to achieve pure collagen matrices that would present both mechanical properties near that of tendon and colonizable by cells.

Conclusion

Our study shows that highly structured collagen core-shell threads favor the differentiation of C3H10T1/2 mesenchymal stem cells into tenocytes. These threads are made by extrusion into a PBS5X buffer of collagen solutions concentrated up to 30 or 60 mg/mL. They are constituted of collagen fibrils which orientations vary at the core-shell interface due to the combined effects of extrusion, viscosity and fibrillogenesis process. After three weeks in culture, C3H10T1/2 cells cover both types of threads and also penetrate over a distance of 30 µm depth into the 30 mg/mL threads. Cells show a strong differentiation into tenocyte, whether in the sheath around the threads or penetrated in it. Cell-seeded collagen threads exhibit a relatively high Young's modulus of 1.11 ± 0.30 MPa at 60 mg/mL in absence of any

post synthetizing treatment. Those results open up new avenues for optimizing tissue engineering scaffolds for tendon regeneration.

Associated Content

SI Supporting Information

Protocol of cell culture on collagen threads under tension, SEM images of threads surfaces at the three concentrations, SHG imaging of the full thickness of collagen threads at 60 mg/mL, C3H10T1/2 cell orientation assessment by means of Orientation J distribution analysis of actin filaments observed with 2PEF microscopy, *in situ* hybridization on collagen 30 and 60 mg/mL threads full cross-sections , Scleraxis, collagen Ia1 and tenomodulin gene expression on 30 mg/mL collagen threads at 1-, 2- and 3-weeks culture, TEM images of cross-sections of collagen threads after 2 weeks in PBS 5X or DMEM at 37°C.

Acknowledgements

Lise Picaut was supported by a PhD grant of the Ecole doctorale 397 (Physique et Chimie des Matériaux) from MESR. This work was partly supported by the Agence Nationale de la Recherche (contracts ANR-10-INBS-04 France BioImaging and ANR-11-EQPX-0029 Morphoscope2). The authors thank Thibaud Coradin for the final touch of the article as well as reviewers for constructive comments.

REFERENCES

(1) Screen, H. R. C.; Berk, D. E.; Kadler, K. E.; Ramirez, F.; Young, M. F. Tendon Functional Extracellular Matrix. *J. Orthop. Res. Off. Publ. Orthop. Res. Soc.* **2015**, *33* (6), 793–799. https://doi.org/10.1002/jor.22818.

(2) Riley, G. Tendinopathy--from Basic Science to Treatment. *Nat. Clin. Pract. Rheumatol.* **2008**, *4* (2), 82–89. https://doi.org/10.1038/ncprheum0700.

(3) Sun, C.; Zhuo, Q.; Chai, W.; Chen, J.; Yang, W.; Tang, P.; Wang, Y. Conservative Interventions for Treating Achilles Tendon Ruptures. In *The Cochrane Library*; John Wiley & Sons, Ltd, 2017. https://doi.org/10.1002/14651858.CD010765.pub2.

(4) Andarawis-Puri, N.; Flatow, E. L.; Soslowsky, L. J. Tendon Basic Science: Development, Repair, Regeneration, and Healing. *J. Orthop. Res. Off. Publ. Orthop. Res. Soc.* **2015**, *33* (6), 780–784. https://doi.org/10.1002/jor.22869.

(5) Rawson, S.; Cartmell, S.; Wong, J. Suture Techniques for Tendon Repair; a Comparative Review. *Muscles Ligaments Tendons J.* **2013**, *3* (3), 220–228.

(6) Rieu, C.; Picaut, L.; Mosser, G.; Trichet, L. From Tendon Injury to Collagen-Based Tendon Regeneration: Overview and Recent Advances. *Curr. Pharm. Des.* **2017**, *23* (24), 3483–3506.

https://doi.org/10.2174/1381612823666170516130515.

(7) El Shewy, M. T.; El Barbary, H. M.; Abdel-Ghani, H. Repair of Chronic Rupture of the Achilles Tendon Using 2 Intratendinous Flaps from the Proximal Gastrocnemius-Soleus Complex. *Am. J. Sports Med.* **2009**, *37* (8), 1570–1577. https://doi.org/10.1177/0363546509333009.

(8) Comley, A. S.; Krishnan, J. Donor Site Morbidity after Quadriceps Tendon Harvest for Rotator Cuff Repair. *Aust. N. Z. J. Surg.* **1999**, *69* (11), 808–810.

(9) Sahoo, S. Chapter 9 - Biologic- and Synthetic-Based Scaffolds for Tendon Regeneration. In *Tendon Regeneration*; Academic Press: Boston, 2015; pp 243–255. https://doi.org/10.1016/B978-0-12-801590-2.00009-0.

(10) Nowotny, J.; Aibibu, D.; Farack, J.; Nimtschke, U.; Hild, M.; Gelinsky, M.; Kasten, P.; Cherif, C. Novel Fiber-Based Pure Chitosan Scaffold for Tendon Augmentation: Biomechanical and Cell Biological Evaluation. *J. Biomater. Sci. Polym. Ed.* **2016**, *27* (10), 917–936. https://doi.org/10.1080/09205063.2016.1155879.

(11) Cavallaro, J. F.; Kemp, P. D.; Kraus, K. H. Collagen Fabrics as Biomaterials. *Biotechnol. Bioeng.* **1994**, *43* (8), 781–791. https://doi.org/10.1002/bit.260430813.

(12) Kew, S. J.; Gwynne, J. H.; Enea, D.; Abu-Rub, M.; Pandit, A.; Zeugolis, D.; Brooks, R. A.; Rushton, N.; Best, S. M.; Cameron, R. E. Regeneration and Repair of Tendon and Ligament Tissue Using Collagen Fibre Biomaterials. *Acta Biomater.* **2011**, *7* (9), 3237–3247. https://doi.org/10.1016/j.actbio.2011.06.002.

(13) Calejo, I.; Costa-Almeida, R.; Reis, R. L.; Gomes, M. E. A Textile Platform Using Continuous Aligned and Textured Composite Microfibers to Engineer Tendon-to-Bone Interface Gradient Scaffolds. *Adv. Healthc. Mater.* **2019**, *8* (15), 1900200. https://doi.org/10.1002/adhm.201900200.

(14) Altman, G. H.; Horan, R. L.; Lu, H. H.; Moreau, J.; Martin, I.; Richmond, J. C.; Kaplan, D. L. Silk Matrix for Tissue Engineered Anterior Cruciate Ligaments. *Biomaterials* **2002**, *23* (20), 4131–4141.

(15) Nakanishi, Y.; Okada, T.; Takeuchi, N.; Kozono, N.; Senju, T.; Nakayama, K.; Nakashima, Y. Histological Evaluation of Tendon Formation Using a Scaffold-Free Three-Dimensional-Bioprinted Construct of Human Dermal Fibroblasts under in Vitro Static Tensile Culture. *Regen. Ther.* **2019**, *11*, 47–55. https://doi.org/10.1016/j.reth.2019.02.002.

(16) Li, W.; Midgley, A. C.; Bai, Y.; Zhu, M.; Chang, H.; Zhu, W.; Wang, L.; Wang, Y.; Wang, H.; Kong, D. Subcutaneously Engineered Autologous Extracellular Matrix Scaffolds with Aligned Microchannels for Enhanced Tendon Regeneration. *Biomaterials* **2019**, *224*, 119488. https://doi.org/10.1016/j.biomaterials.2019.119488.

(17) Meyer, M. Processing of Collagen Based Biomaterials and the Resulting Materials Properties. *Biomed. Eng. OnLine* **2019**, *18* (1). https://doi.org/10.1186/s12938-019-0647-0.

(18) Yang, S.; Shi, X.; Li, X.; Wang, J.; Wang, Y.; Luo, Y. Oriented Collagen Fiber Membranes Formed through Counter-Rotating Extrusion and Their Application in Tendon Regeneration. *Biomaterials* **2019**, *207*, 61–75. https://doi.org/10.1016/j.biomaterials.2019.03.041.

(19) Cheng, X.; Gurkan, U. A.; Dehen, C. J.; Tate, M. P.; Hillhouse, H. W.; Simpson, G. J.; Akkus,

O. An Electrochemical Fabrication Process for the Assembly of Anisotropically Oriented Collagen Bundles. *Biomaterials* **2008**, *29* (22), 3278–3288. https://doi.org/10.1016/j.biomaterials.2008.04.028.

(20) Lode, A.; Meyer, M.; Brüggemeier, S.; Paul, B.; Baltzer, H.; Schröpfer, M.; Winkelmann, C.; Sonntag, F.; Gelinsky, M. Additive Manufacturing of Collagen Scaffolds by Three-Dimensional Plotting of Highly Viscous Dispersions. *Biofabrication* **2016**, *8* (1), 015015. https://doi.org/10.1088/1758-5090/8/1/015015.

(21) Rieu, C.; Parisi, C.; Mosser, G.; Haye, B.; Coradin, T.; Fernandes, F. M.; Trichet, L. Topotactic Fibrillogenesis of Freeze-Cast Microridged Collagen Scaffolds for 3D Cell Culture. *ACS Appl. Mater. Interfaces* **2019**, *11* (16), 14672–14683. https://doi.org/10.1021/acsami.9b03219.

(22) Laurent, C. P.; Durville, D.; Mainard, D.; Ganghoffer, J.-F.; Rahouadj, R. A Multilayer Braided Scaffold for Anterior Cruciate Ligament: Mechanical Modeling at the Fiber Scale. *J. Mech. Behav. Biomed. Mater.* **2012**, *12*, 184–196. https://doi.org/10.1016/j.jmbbm.2012.03.005.

(23) Daamen, W. F.; Nillesen, S. T. M.; Hafmans, T.; Veerkamp, J. H.; van Luyn, M. J. A.; van Kuppevelt, T. H. Tissue Response of Defined Collagen–Elastin Scaffolds in Young and Adult Rats with Special Attention to Calcification. *Biomaterials* **2005**, *26* (1), 81–92. https://doi.org/10.1016/j.biomaterials.2004.02.011.

(24) Helary, C.; Abed, A.; Mosser, G.; Louedec, L.; Letourneur, D.; Coradin, T.; Giraud-Guille, M. M.; Meddahi-Pellé, A. Evaluation of Dense Collagen Matrices as Medicated Wound Dressing for the Treatment of Cutaneous Chronic Wounds. *Biomater Sci* **2015**, *3* (2), 373–382. https://doi.org/10.1039/C4BM00370E.

(25) Vigier, S.; Catania, C.; Baroukh, B.; Saffar, J.-L.; Giraud-Guille, M.-M.; Colombier, M.-L. Dense Fibrillar Collagen Matrices Sustain Osteoblast Phenotype In Vitro and Promote Bone Formation in Rat Calvaria Defect. *Tissue Engineering*. 2011, pp 889–898.

(26) Picaut, L.; Trichet, L.; Ronsin, O.; Haye, B.; Génois, I.; Baumberger, T.; Mosser, G. Pure Dense Collagen Threads from Extrusion to Fibrillogenesis Stability. *Biomed. Phys. Eng. Express* **2018**. https://doi.org/10.1088/2057-1976/aaab78.

(27) Picaut, L.; Ronsin, O.; Caroli, C.; Baumberger, T. Experimental Evidence of a Helical, Supercritical Instability in Pipe Flow of Shear Thinning Fluids. *Phys. Rev. Fluids* **2017**, *2* (8), 083303. https://doi.org/10.1103/PhysRevFluids.2.083303.

(28) Reznikoff, C. A.; Brankow, D. W.; Heidelberger, C. Establishment and Characterization of a Cloned Line of C3H Mouse Embryo Cells Sensitive to Postconfluence Inhibition of Division. **1973**, *33*, 9.

(29) Kapacee, Z.; Richardson, S. H.; Lu, Y.; Starborg, T.; Holmes, D. F.; Baar, K.; Kadler, K. E. Tension Is Required for Fibripositor Formation. *Matrix Biol.* **2008**, *27* (4), 371–375. https://doi.org/10.1016/j.matbio.2007.11.006.

(30) Bonnin, M.-A.; Laclef, C.; Blaise, R.; Eloy-Trinquet, S.; Relaix, F.; Maire, P.; Duprez, D. Six1 Is Not Involved in Limb Tendon Development, but Is Expressed in Limb Connective Tissue under Shh Regulation. *Mech. Dev.* **2005**, *122* (4), 573–585. https://doi.org/10.1016/j.mod.2004.11.005.

(31) Havis, E.; Coumailleau, P.; Bonnet, A.; Bismuth, K.; Bonnin, M.-A.; Johnson, R.; Fan, C.-M.; Relaix, F.; Shi, D.-L.; Duprez, D. Sim2 Prevents Entry into the Myogenic Program by Repressing

MyoD Transcription during Limb Embryonic Myogenesis. *Dev. Camb. Engl.* **2012**, *139* (11), 1910–1920. https://doi.org/10.1242/dev.072561.

(32) Lejard, V.; Blais, F.; Guerquin, M.-J.; Bonnet, A.; Bonnin, M.-A.; Havis, E.; Malbouyres, M.; Bidaud, C. B.; Maro, G.; Gilardi-Hebenstreit, P.; Rossert, J.; Ruggiero, F.; Duprez, D. EGR1 and EGR2 Involvement in Vertebrate Tendon Differentiation. *J. Biol. Chem.* **2011**, *286* (7), 5855–5867. https://doi.org/10.1074/jbc.M110.153106.

(33) Havis, E.; Bonnin, M.-A.; Olivera-Martinez, I.; Nazaret, N.; Ruggiu, M.; Weibel, J.; Durand, C.; Guerquin, M.-J.; Bonod-Bidaud, C.; Ruggiero, F.; Schweitzer, R.; Duprez, D. Transcriptomic Analysis of Mouse Limb Tendon Cells during Development. *Development* **2014**, *141* (19), 3683–3696. https://doi.org/10.1242/dev.108654.

(34) Teulon, C.; Tidu, A.; Portier, F.; Mosser, G.; Schanne-Klein, M.-C. Probing the 3D Structure of Cornea-like Collagen Liquid Crystals with Polarization-Resolved SHG Microscopy. *Opt. Express* **2016**, *24* (14), 16084–16098. https://doi.org/10.1364/OE.24.016084.

(35) Larson, R. G. Instabilities in Viscoelastic Flows. *Rheol. Acta* **1992**, *31* (3), 213–263. https://doi.org/10.1007/BF00366504.

(36) Gaut, L.; Duprez, D. Tendon Development and Diseases. *Wiley Interdiscip. Rev. Dev. Biol. 5* (1), 5–23. https://doi.org/10.1002/wdev.201.

(37) Kato, Y. P.; Christiansen, D. L.; Hahn, R. A.; Shieh, S.-J.; Goldstein, J. D.; Silver, F. H. Mechanical Properties of Collagen Fibres: A Comparison of Reconstituted and Rat Tail Tendon Fibres. *Biomaterials* **1989**, *10* (1), 38–42. https://doi.org/10.1016/0142-9612(89)90007-0.

(38) Cornwell, K. G.; Lei, P.; Andreadis, S. T.; Pins, G. D. Crosslinking of Discrete Self-Assembled Collagen Threads: Effects on Mechanical Strength and Cell–Matrix Interactions. *J. Biomed. Mater. Res. A* **2007**, *80A* (2), 362–371. https://doi.org/10.1002/jbm.a.30893.

(39) Tidu, A.; Ghoubay-Benallaoua, D.; Teulon, C.; Asnacios, S.; Grieve, K.; Portier, F.; Schanne-Klein, M.-C.; Borderie, V.; Mosser, G. Highly Concentrated Collagen Solutions Leading to Transparent Scaffolds of Controlled Three-Dimensional Organizations for Corneal Epithelial Cell Colonization. *Biomater. Sci.* **2018**, *6* (6), 1492–1502. https://doi.org/10.1039/C7BM01163F.

(40) Gobeaux, F.; Belamie, E.; Mosser, G.; Davidson, P.; Asnacios, S. Power Law Rheology and Strain-Induced Yielding in Acidic Solutions of Type I-Collagen. *Soft Matter* **2010**, *6* (16), 3769–3777. https://doi.org/10.1039/B922151D.

(41) Picaut, L. *Synthèse d'un Tendon Artificiel*; Paris 6, 2017.

(42) Kuo, C. K.; Tuan, R. S. Mechanoactive Tenogenic Differentiation of Human Mesenchymal Stem Cells. *Tissue Eng. Part A* **2008**, *14* (10), 1615–1627. https://doi.org/10.1089/ten.tea.2006.0415.

(43) Werner, M.; Blanquer, S. B. G.; Haimi, S. P.; Korus, G.; Dunlop, J. W. C.; Duda, G. N.; Grijpma, D. W.; Petersen, A. Surface Curvature Differentially Regulates Stem Cell Migration and Differentiation via Altered Attachment Morphology and Nuclear Deformation. *Adv. Sci. Weinh. Baden-Wurtt. Ger.* **2017**, *4* (2), 1600347. https://doi.org/10.1002/advs.201600347.

(44) Helary, C.; Ovtracht, L.; Coulomb, B.; Godeau, G.; Giraud-Guille, M. M. Dense Fibrillar Collagen Matrices: A Model to Study Myofibroblast Behaviour during Wound Healing. *Biomaterials*

2006, *27* (25), 4443–4452. https://doi.org/10.1016/j.biomaterials.2006.04.005.

(45) Gaut, L.; Bonnin, M.-A.; Blavet, C.; Cacciapuoti, I.; Orpel, M.; Mericskay, M.; Duprez, D. Mechanical and Molecular Parameters That Influence the Tendon Differentiation Potential of C3H10T1/2 Cells in 2D- and 3D-Culture Systems. *Biol. Open* **2020**, *9* (2), bio047928. https://doi.org/10.1242/bio.047928.

(46) Kim, W. J.; Yun, H.-S.; Kim, G. H. An Innovative Cell-Laden α-TCP/Collagen Scaffold Fabricated Using a Two-Step Printing Process for Potential Application in Regenerating Hard Tissues. *Sci. Rep.* **2017**, *7* (1), 3181. https://doi.org/10.1038/s41598-017-03455-9.

(47) Chen, X.; Yin, Z.; Chen, J.; Shen, W.; Liu, H.; Tang, Q.; Fang, Z.; Lu, L.; Ji, J.; Ouyang, H. Force and Scleraxis Synergistically Promote the Commitment of Human ES Cells Derived MSCs to Tenocytes. *Sci. Rep.* **2012**, *2* (1), 977. https://doi.org/10.1038/srep00977.

(48) Gentleman, E.; Lay, A. N.; Dickerson, D. A.; Nauman, E. A.; Livesay, G. A.; Dee, K. C. Mechanical Characterization of Collagen Fibers and Scaffolds for Tissue Engineering. *Biomaterials* **2003**, *24* (21), 3805–3813. https://doi.org/10.1016/S0142-9612(03)00206-0.

For Table of Contents Use Only

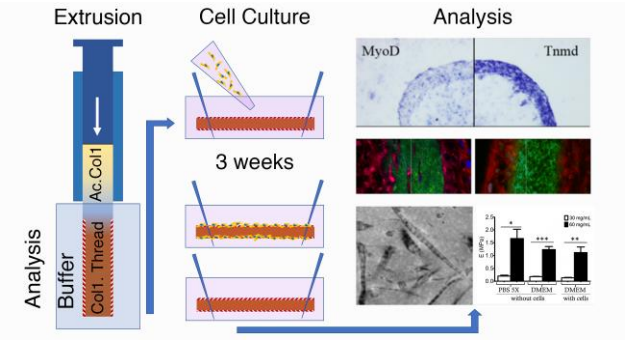

Core-shell pure collagen threads extruded from highly concentrated solutions promote colonization and differentiation of C3H10T1/2 cells

Authors: Lise Picaut[1,2], Léa Trichet[2], Christophe Hélary[2], Guillaume Ducourthial[3], Marie-Ange Bonnin[4], Bernard Haye[2], Olivier Ronsin[1], Marie-Claire Schanne-Klein[3], Delphine Duprez[4], Tristan Baumberger[1] and Gervaise Mosser[2].